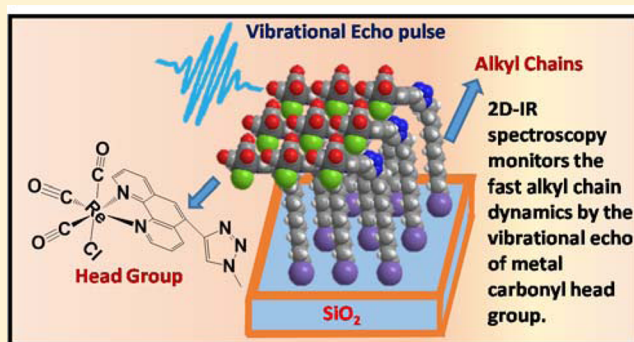# Structural Influences on the Fast Dynamics of Alkylsiloxane Monolayers on SiO$_2$ Surfaces Measured with 2D IR Spectroscopy

Chang Yan, Rongfeng Yuan, Jun Nishida, and Michael D. Fayer*

Department of Chemistry, Stanford University, Stanford, California 94305, United States

Ⓢ Supporting Information

ABSTRACT: There is widespread interest in alkyl chain surface monolayers and their applications. In many applications, alkyl monolayers are functionalized with active head-groups. Here we report the impact of major structural variations on the fast dynamics of alkylsiloxane monolayers. The monolayers were deposited with controlled structures on flat amorphous silica surfaces, and the terminal sites were functionalized with a metal carbonyl headgroup. The CO symmetric stretching mode of the headgroup served as a vibrational probe for detecting the fast structural dynamics of the monolayers using two-dimensional infrared vibrational echo spectroscopy (2D IR) to measure spectral diffusion, which is made quantitative by determining the frequency–frequency correlation function (FFCF) from the time-dependent data. Two methods of functionalizing the surface, independent attachment via a single Si–O bond formed with alkylmonochlorosilane precursors and network attachment via siloxane networks (–Si–O–Si–O–) formed with alkyltrichlorosilane precursors, were compared for several chain lengths. The two types of monolayers produced chain dynamics and structures that were independent of the manner of attachment. For densely packed monolayers, the FFCF decayed mildly slower when the alkyl chain length was decreased from C11 (chain with 11 methylenes) to C4. However, when the chain length was further reduced by one more methylene to C3, substantially slower dynamics were observed. When the chain density was reduced below 50% of fully packed monolayers, the single-component nature of the dynamics changed to a fast component plus an extremely slow component, possibly because of the collapse and entanglement of loosely packed alkyl chains.

1. INTRODUCTION

There is considerable interest in the investigation of two-dimensional (2D) materials[1,2] because their physical properties are distinct from those of bulk systems. One class of 2D systems that has received a great deal of attention is a single layer of alkyl chains assembled on a flat substrate, i.e., alkyl monolayers.[3] Alkyl monolayers can form on a variety of surfaces, e.g., a Langmuir–Blodgett film on a water surface,[4] an alkylthiolate monolayer on a gold surface,[5] and an alkylsiloxane monolayer on a planar silica surface.

Alkylsiloxane monolayers have alkyl chains bound to a flat silica substrate via Si–O bonds.[6] Depending on the specific composition of the alkyl chains, alkylsiloxane monolayers can have diverse structures with a wide range of properties. The surface of the monolayers (chain ends away from the substrate) can be modified by various functional groups, giving rise to a range of tunable surface properties.[7] Functionalized alkyl monolayers have found applications in fields such as surface protection,[8] self-cleaning,[9] surface recognition of molecules,[10] oriented growth of crystals at interfaces,[11] enhanced catalytic activity,[12] cell adhesion,[13] protein arrays,[14] and organic transistors.[15]

The diverse but relatively ordered nature of alkylsiloxane monolayers has allowed their static structures to be extensively studied using a variety of methods. These methods include ellipsometry,[16] linear absorption spectroscopy,[17] sum-frequency generation (SFG) spectroscopy,[18] X-ray photoelectron spectroscopy,[19] and scanning probe microscopy.[20] In contrast to the extensive characterization of static structures, there have been fewer studies that directly investigate the fast structural dynamics of alkyl monolayers on planar surfaces. The challenge is to apply a technique that can probe the weak signal from a monolayer surface while operating on a sufficiently fast time scale (picoseconds).

SFG spectroscopy is inherently interface selective, and is used to separate an interface signal from a bulk solvent. The methodology for extracting static structural information from SFG experiments, in particular the orientations of interfacial molecules, has been applied to a variety of systems, including alkyl monolayers.[21−23] SFG can also be used to make fast time-dependent measurements of dynamics at interfaces by combining it with vibrational pump–probe or two-dimensional

infrared (2D IR) spectroscopy. The vibrational pump−probe SFG experiments can provide vibrational lifetimes and information on orientation relaxation, although the quantitative analysis of the data can be complicated.[21,24] Notable examples of the application of time-resolved SFG include the dynamics at the water/air interface,[25,26] the dynamics of carbon monoxide adsorbed on a platinum surface,[27] and the dynamics of peptides on a gold surface.[28]

Time-resolved SFG methods have been applied to study the influence of shock waves on alkyl monolayers. Dlott and co-workers applied a shock wave followed by a variable time-delayed SFG probe to alkylthiolate monolayers on gold and observed the shock-induced dynamics of the monolayer.[29] Bonn and co-workers measured the vibrational lifetime and coupling among modes in Langmuir monolayers using 2D IR SFG spectroscopy.[30] SFG-FID spectroscopy was used to measure the free induction decay (FID) of methyl and methylene groups in alkyl monolayers.[31,32] The Fourier transform of the FID gives the time-independent vibrational spectrum. Benderskii and co-workers estimated the time scale of the rotational dynamics of methyl groups on Si(111) surfaces by line width analysis of polarization-selective SFG spectra.[33]

Another approach for studying the fast structural dynamics of monolayers on a surface is to place a probe in the monolayer that can generate a strong signal using a non-interface-selective technique to observe the signal. Since the probe is only found in the monolayer, the experiment becomes monolayer specific. For example, pyrene bound to a short alkyl chain embedded in a monolayer of longer chains was used in time-correlated single-photon-counting fluorescence anisotropy experiments to observe the restricted anisotropy decay occurring on a multinanosecond time scale.[34]

The utility of experiments that can measure the fast structural dynamics of an alkyl monolayer arises because the chains are in constant motion at room temperature. Although the chains are pinned to the surface, they can undergo tilting, bending, and hindered rotational motions. Such motions will cause head-groups to change position and orientation. In bulk solution, the nature of the solvent and its dynamics can play important roles in chemistry. Solvent fluctuations are responsible for taking a system to a transition state in processes such as chemical reactions and electron transfer. In applications involving functionalized alkyl chain monolayers, the active headgroup frequently sits at the interface between the solvent and the underlying alkyl chains. Then the dynamic interactions of the active moiety with its environment will in part depend on the alkyl chain dynamics.

Molecular dynamics (MD) simulations of 15 or 14 methylene alkyl chains terminated with methyl groups and bound to crystalline gold with thiolate linkages have been presented.[35−37] These studies focused on structure but also provide information on chain dynamics. Initially two models were used that only differed by the manner of attachment of the chains to the gold surface.[35] Orientational dynamics of ∼5 ps and many tens of picoseconds were obtained depending on the manner of attachment. Later simulations showed orientational dynamics on the many tens of picoseconds time scale.[37]

Structural dynamics are often accompanied by time-dependent changes of vibrational frequencies, which are influenced by structural and chemical environments. The time evolution of vibrational frequencies, which is caused by structural evolution of the vibrational oscillators' environments, is called spectral diffusion. 2D IR spectroscopy measures spectral diffusion, and

therefore can be used to study fast dynamics in condensed matter systems under thermal equilibrium conditions.[38,39] Examples of systems and processes that have been explicated using 2D IR spectroscopy include the dynamics of solvent−solute complexes in organic solutions,[40] ultrafast tautomerization dynamics,[41] conformation dynamics of macromolecules,[42] dynamics of metal carbonyl complexes at a transition state[43] and an excited state,[44] dynamics of ice,[45] structures of peptides and proteins,[46,47] and water dynamics at interfaces or in bulk and confined environments.[48−50]

Recently 2D IR vibrational echo spectroscopy has been applied to study the structural dynamics of alkyl chain monolayers on amorphous silica[51−54] and crystalline gold surfaces.[55] In the experimental study presented here, we examined a number of alkyl chain systems on planar amorphous silica surfaces by 2D IR spectroscopy to understand the influence of the chain properties on their structural dynamics under thermal equilibrium conditions at room temperature. The chains were functionalized with a metal carbonyl headgroup, which serves as the monolayer-specific vibrational probe that reports on the chain dynamics, and it also mimics an active headgroup moiety that is present in many applications. We address three questions: (1) Does the manner of chain attachment to the silica surface affect the chain dynamics? (2) To what extent do the lengths of the alkyl chains influence the chain dynamics? (3) How does the density of chains on the surface change the chain dynamics?

To answer these questions, a variety of samples with different alkyl chain structures were prepared and studied with 2D IR experiments to observe the influence of the monolayer structure on the alkyl chain dynamics. First, to address the effect of the manner of chain attachment to the surface, two attachment methods were employed. Independent chains were attached directly to the silica surface by a single Si−O bond using alkylmonochlorosilane as the precursor. The dynamics of these monolayers were compared to those of monolayers prepared with trichlorosilane precursors. The trichlorosilanes react in solution with each other to form a polymeric network (−Si−O−Si−O−) that then attaches to the substrate via the remaining unreacted chloro groups. For these samples, the alkyl chains emanate from the network layer that is itself bound to the substrate. Second, the influence of the alkyl chain length was studied by measuring spectral diffusion for alkyl chains with different lengths, C11, C4, and C3, where the number is the number of methylenes. Finally, the influence of the chain density was studied by preparing samples ranging from maximum coverage to ∼15% of the maximum chain density. The experimental results provide answers to the three questions.

To achieve the necessary sensitivity to observe the dynamics of surface monolayers, a vibrational probe with a large transition dipole was employed, i.e., a rhenium tricarbonyl complex, *fac*-tricarbonylchloro(1,10-phenanthroline)rhenium-(I), referred to as RePhen(CO)$_3$Cl. RePhen(CO)$_3$Cl was attached to the end of the alkyl chains away from the surface. The CO symmetric stretching mode has a strong vibrational transition, and its absorption frequency is well-separated from other vibrational modes of the rest of the sample. These factors made it possible to obtain surface-specific 2D IR spectra with good signal-to-noise ratios.[52,53] The spectral diffusion of the RePhen(CO)$_3$Cl headgroup reported on the dynamics of the alkyl chains. In addition, the carbonyl symmetric stretch has a reasonably long vibrational lifetime (∼20 ps), which made it

possible to observe the dynamics from <1 to ~75 ps. This range of times allowed relatively small differences in the structural dynamics in alkylsiloxane monolayers to be observed.[54]

2. EXPERIMENTAL METHODS

2.1. Sample Fabrication. To avoid absorption of the mid-infrared radiation by the silica substrate, the alkyl monolayers were grown on a SiO_2/CaF_2 substrate. A 100 nm thick silica layer was deposited on a 3 mm thick CaF_2 optical window (1 in. in diameter). The SiO_2/CaF_2 substrates were prepared by a plasma-enhanced chemical vapor deposition procedure described previously.[54] To deposit monolayers of good quality without forming multilayers, we followed the well-established method of immersing the substrates in a dilute solution of bromoalkylchlorosilanes.[56−58] After deposition, the terminal bromine atom was replaced by an azide group by a nucleophilic substitution. Finally the metal carbonyl vibrational probe, *fac*-tricarbonylchloro(1,10-phenanthroline)rhenium(I), was "clicked" on by the copper-catalyzed azide−alkyne cyclo-addition (CuAAC).[59] The entire headgroup (Figure 1A) consists of the $RePhen(CO)_3Cl$ and the triazole ring formed during the "click" chemistry. The details of synthesis for each kind of monolayer sample can be found in the Supporting Information.

2.2. Infrared Absorption Spectroscopy and Inductively Coupled Plasma Mass Spectrometry. Unpolarized and polarization-resolved infrared absorption measurements were applied with inductively coupled plasma mass spectrometry (ICP-MS) to determine the structure, headgroup orientation, and surface density of the functionalized monolayer samples. The FT-IR spectra of the monolayers were recorded with 1 cm^{-1} resolution. Monolayers were cleaned by sonication with ethanol, and then the spectra were immediately measured. Multiple cleaning cycles in ethanol caused no change in the FT-IR or 2D IR results. We measured the absorption spectra with an unpolarized beam at an incident angle of 0° using air free of CO_2 and water vapor as the background. For polarization-resolved spectra, both s- and p-polarized spectra were taken for each monolayer sample at an incident angle of 45° to the surface using a bare SiO_2/CaF_2 wafer as the background. The usage of the wafer as the background was to account for the difference in reflectivity for the s- and p-polarized beams.

The methodology for determining the transition dipole moment orientation of a surface-bound vibrational mode by polarization-resolved infrared absorption spectroscopy had been described previously.[51,52] We define θ as the polar angle between the transition dipole moment of the carbonyl symmetric stretching mode and the surface normal to the substrate. Since the alkylsiloxane monolayers do not have long-range orientational correlation, the azimuthal angle of the transition dipole moment is randomly distributed from 0 to 2π. From eq 1 below, we can obtain the averaged orientational order parameter of the transition dipole moment. Assuming a narrowly peaked distribution of orientations (relatively small cone of angles), the angle θ can be extracted from the order parameter using eq 2 (see the Supporting Information).

$$\frac{A_s}{A_p} = \left(1 + \frac{3\langle S \rangle \sin^2 \alpha}{1 - \langle S \rangle}\right)^{-1} \tag{1}$$

$$\langle S \rangle = 1/2(3\langle \cos^2 \theta \rangle - 1) \tag{2}$$

A_s and A_p are the peak areas of s- and p-polarized spectra. $\langle S \rangle$ is the averaged orientational order parameter. α is the beam's incident angle.

Using the transition dipole moment orientation and the integrated extinction coefficient, we can determine the surface density of the monolayer headgroups, Γ_{surf} (molecules/cm^2). The extinction coefficient of the metal carbonyl headgroup was shown to be sensitive to subtle changes in chemical environments such as surrounding solvent molecules.[53] Therefore, the extinction coefficient on a bare monolayer surface exposed to air could differ from the value of bulk solutions by a significant amount. To calibrate the extinction coefficient, we directly determined the total amount of rhenium on the surface for C4 monolayer samples by ICP-MS analysis.[51] The accuracy of the measurement stems from the high sensitivity of ICP-MS and the ultralow natural abundance of rhenium. ε_{surf} is the integrated molar extinction coefficient of the carbonyl symmetric stretching mode at the monolayer/air interface with the energy axis in inverse centimeters. Using the ICP-MS results and eq 3, ε_{surf} was determined to be 7.90×10^6 cm mol^{-1}.

$$\Gamma_{surf} = N_A \frac{A_{unp}}{\varepsilon_{surf} R} \tag{3}$$

Γ_{surf} is the surface density of headgroups, A_{unp} is the peak area of the unpolarized spectra, N_A is Avogadro's constant, and $R = (3/2) \sin^2 \theta$ is the correction factor to account for the difference between isotropic absorption and anisotropic absorption. This extinction coefficient and eq 3 were used for calculating the surface density of headgroups for other monolayer samples.

2.3. 2D IR and HDTG Measurements. Both 2D IR and HDTG (heterodyne-detected transient grating) spectroscopies were performed under BOXCARS geometry on the same optical platform. Midinfrared pulses with a duration of ~170 fs, bandwidth of 90 cm^{-1}, pulse energy of ~5.5 μJ, and center at ~2025 cm^{-1} were generated at 1 kHz with an optical parametric amplifier pumped by a regeneratively amplified Ti:sapphire system. The infrared pulses selectively pumped the carbonyl symmetric stretching mode without exciting other modes. The echo signal pulse was combined with an external local oscillator (LO) pulse for heterodyne detection. The combined pulse passed through a monochromator equipped with a liquid N_2 cooled 32 pixel HgCdTe (MCT) array detector.

2D IR and HDTG spectroscopies are both third-order nonlinear time-resolved experiments. The theory and experimental design have been described in detail previously;[52,60] a brief description is given here. Three infrared pulses (denoted as pulses 1, 2, and 3 in temporal sequence) that selectively excite the carbonyl symmetric stretching mode are focused and overlapped spatially on the monolayer surface. The time period between pulse 1 and pulse 2 is denoted as τ, and the time period between pulse 2 and pulse 3 is denoted as T_w. These temporal intervals are controlled by precision delay lines. The interaction of the three pulses with the sample leads to the emission of an echo pulse in the wave-vector-matched direction.

2D IR spectroscopy probes the dynamics of a chemical system by measuring spectral diffusion, which is the time evolution of the vibrational frequencies of the probe vibration. The vibrational absorption line is inhomogeneously broadened

because of the range of intermolecular interactions of the vibrational probes with their surroundings. The change in frequencies with time (spectral diffusion) is caused by the structural fluctuations of the sample. Qualitatively, the experiment works as follows: In effect, the first pulse of the vibrational echo pulse sequence "labels" the initial vibrational probe frequencies (the ω_τ horizontal axis in the 2D spectrum), and the second pulse stores the information. Then, during T_w, the waiting time between pulses 2 and 3, the structure of the monolayer evolves, causing the vibrational frequencies to change. This period is ended by the arrival of the third pulse, which also stimulates the emission of the vibrational echo pulse. The echo contains information on the final frequencies of the vibrational oscillators (the ω_m vertical axis in the 2D spectrum). When T_w is short, the structure of the monolayer is relatively unchanged from when the vibrations were first labeled, producing final frequencies that differ little from the starting frequencies. At longer T_w, the monolayer structure has had more time to evolve, and the final frequencies are less correlated with the initial frequencies. The loss of correlation as T_w increases is manifested as a change in the shape of the 2D IR spectrum. At short T_w, the 2D IR spectrum is elongated along the diagonal (the 45° line with positive slope that bisects the vertical and horizontal frequency axes). As T_w increases and frequencies are less correlated, the shape of the spectrum becomes more circular. If all of the environments are sampled within the experimental time window, which is limited by the vibrational lifetime, the spectrum becomes round. Thus, the structural dynamics of the monolayer, that is, the alkyl chain dynamics, can be obtained from the change in the shape of the 2D IR spectra as a function of T_w.

Quantitatively, the dynamical information is extracted from these 2D line shape changes via the center line slope (CLS) technique, which has been shown to be the equivalent of the normalized frequency−frequency correlation function (FFCF).[61,62] The CLS provides the time constants for the various components of the spectral diffusion and their relative amplitudes. In the CLS decay, the deviation from 1 at $T_w = 0$ is a normalized measure of the homogeneous line width. A wider homogeneous line width produces a larger deviation from 1 for the initial value of the CLS.[61,62] Combining the CLS data with the linear absorption spectrum yields the FFCF, including the homogeneous dephasing contribution to the absorption spectrum and the absolute amplitudes of the spectral diffusion components. The time constants in the CLS and the FFCF are the same.[61,62]

The FFCF can be written as a sum of exponentials:

$$C(t) = \langle \delta\omega(t)\, \delta\omega(0) \rangle = \sum_i \Delta_i^{\,2} \exp(-t/\tau_i) \tag{4}$$

Here $\delta\omega(t) = \omega(t) - \langle\omega\rangle$ is the instantaneous frequency fluctuation, Δ_i is the frequency fluctuation amplitude of the ith inhomogeneous contribution to the line shape, and τ_i is the correlation time of component i (equal to the ith exponential time constant from the CLS decay). If one of the components of the frequency fluctuations meets the condition $\Delta_i \tau_i < 1$, the component is motionally narrowed. In this case, Δ_i and τ_i cannot be determined separately, and a homogeneous component with pure dephasing line width $\Gamma^* = \Delta_i^{\,2}\tau_i = 1/(\pi T_2^*)$ contributes to the FFCF. $T_2 = 1/(\pi\Gamma)$ is the total homogeneous dephasing time (with Γ the homogeneous line width). The total homogeneous dephasing time is given by

$$\frac{1}{T_2} = \frac{1}{T_2^*} + \frac{1}{2T_1} + \frac{1}{3T_{or}} \tag{5}$$

where T_1 is the vibrational lifetime and T_{or} is the orientational relaxation time. In the surface experiments, the chains are pinned to the surface, and the orientational contribution to the homogeneous line width is negligible. In addition, the vibrational lifetime is long and contributes <0.25 cm^{-1} to the homogeneous line width. Therefore, the homogeneous line widths are dominated by pure dephasing. The total homogeneous dephasing time T_2 and the values of Δ_i in units of frequency are obtained from the experimental data from a simultaneous fit to the CLS decay and the experimental linear absorption line shape.[61,62]

Most of the data presented below are described well by a single-exponential decay for the spectral diffusion part of the normalized FFCF (CLS), which characterizes the sampling of the inhomogeneous portion of the absorption line shape. There is also the homogeneous contribution. We take the exponential time constant(s) to characterize the time scale of the dynamics rather than associating it with a single structural motion. It is important to note that the CLS decay is an experimental observable which is independent of a model of the dynamics. It is therefore amenable to comparison with MD simulations, and does not require using a multiexponential model like that embodied in eq 4. Simulations have been compared to the results of 2D IR experiments for a variety of systems.[48,63−66]

In the HDTG experiment that measures the vibrational lifetime, τ_{VR}, τ is fixed at zero, and only T_w is scanned. The spatial and temporal overlap of pulses 1 and 2 produces an optical interference pattern, i.e., alternating regions of light and dark that produce alternating spatial regions of excited and unexcited molecular vibrations. This sinusoidal variation in the population density of excited states acts as a diffraction grating for the incoming pulse 3.[67−69] The diffracted pulse, which is heterodyne detected in the same manner as the vibrational echo, is the signal. As the vibrations decay to the ground state, the diffraction grating decays, and the signal decays. Because the absorption of the sample is very small (∼0.5 mOD), HDTG spectroscopy was chosen over the pump−probe method for its higher sensitivity.[51] At short time, there is a small contribution to the decay from restricted orientational motions, which can provide additional information.[54] Here only the lifetimes are of interest, which were extracted from the long time portions of the HDTG decays.

3. RESULTS AND DISCUSSION

3.1. Network and Independently Attached Monolayers. In this section the question of possible differences in chain dynamics and structure resulting from two methods of attaching the chains to the amorphous SiO_2 surface are addressed. When monolayers are prepared using trichlorosilanes, e.g., C11−SiCl$_3$, on substrates, the trichlorosilanes react in solution to form an extended polymeric network prior to attachment to the surface.[57] The result is that the chains emanate from interlinked networks at the bottom of the monolayer with the network layer attached to the SiO_2 surface. We denote this type of monolayer as the network monolayer, and use the abbreviation "net". Figure 1B shows a schematic illustration for C11$_{net}$ chains. C4$_{net}$ and C3$_{net}$ were prepared and measured as well. For the detailed structure of the headgroup, refer to Figure 1A. In contrast, when chains are deposited on the substrate using monochlorodimethylsilanes, e.g., C11−
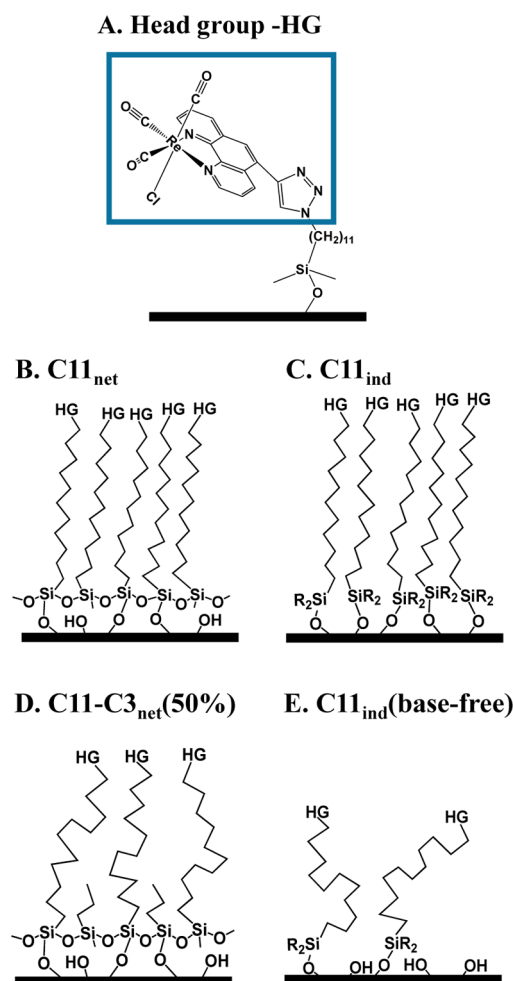
A. Head group -HG

B. C11_net   **C. C11_ind**

D. C11-C3_net(50%)   **E. C11_ind(base-free)**

Figure 1. Schematic illustrations of the functionalized alkylsiloxane monolayers. The −R represents the methyl group, and −HG represents the headgroup. (A) Structure of the headgroup (blue square). (B) C11 monolayers with network attachment. (C) C11 monolayers with independent attachment. (D) Mixed monolayers of 50% C11 and 50% C3 chains with network attachment. (E) C11 monolayers of low chain density (15%) with independent attachment.

$Si(CH_3)_2Cl$, under base conditions, the chains are independently attached to the surface.[58] The base-catalyzed reaction scheme was used to obtain a chain density similar to that of the network monolayers. We refer to these samples as independently attached base catalyzed, and use the abbreviation "ind". An illustration for C11 independently attached chains ($C11_{ind}$) is shown in Figure 1C.

The manner of attachment might influence the chain dynamics because of a difference in the structural flexibility of the material below the alkyl chains. In both attachment methods, the alkyl chains are bound to an Si atom. In the direct attachment, the Si atom is bound to the solid surface, which locally is similar to crystalline SiO_2. While there are phonon modes of the solid as well as surface modes, these modes will not produce significant chain structural motions. In contrast, in the network attachment, the alkyl chains are bound to a nominally two-dimensional layer that is fixed to the surface through sporadic bonds. The 2D network could undergo more substantial structural fluctuations than the SiO_2 solid surface. If the 2D network undergoes buckling or butterfly-type structural changes, such fluctuations could result in chains undergoing up

and down and tilting movements that would not occur with direct attachment to the more structurally rigid solid.

For all of the samples, infrared linear absorption spectra of the C−H region of the alkyl chains give the antisymmetric and symmetric stretching mode frequencies of the methylene ($−CH_2−$) groups at 2854 and 2925 cm^{-1}, respectively. The shift of the symmetric stretching frequency from the all-trans value (2918 cm^{-1}) indicates the existence of gauche defects within the monolayer of alkyl chains, which is normal for alkylsiloxane monolayers.[3,70,71] For the independently attached monolayers, we also detected the very weak absorptions of antisymmetric and symmetric stretching modes of methyl ($−CH_3$) groups at 2873 and 2962 cm^{-1}, from the two methyl groups associated with the silicon atom at the bottom of the alkyl chains.[70,71]

The carbonyl symmetric stretching mode (∼2025 cm^{-1}) and the two antisymmetric stretching modes (∼1921 and 1898 cm^{-1}) of the headgroup were observed for all of the functionalized monolayers. Owing to the large transition dipole, the carbonyl peaks had a larger absorbance (∼0.7 mOD) and smoother line shapes than C−H peaks. We performed all of the time-resolved experiments on the symmetric mode because it is well separated in the spectrum from the two antisymmetric peaks, which overlap substantially and would make data analysis difficult.[51] Table 1 gives time-independent parameters for the symmetric stretching mode. The full width at half-maximum (fwhm) of the absorption spectra of all of the samples is 17−18 cm^{-1}.

Table 1. Infrared Absorption Spectrum Parameters[a]

sample	peak freq (cm^{-1})	fwhm (cm^{-1})	θ (deg)	Γ_{surf} (10^{14} cm^{-2})
$C11_{net}$	2023 ± 0.5	17 ± 0.5	63 ± 3	8.6 ± 0.5
$C4_{net}$	2025 ± 0.5	18 ± 0.5	64 ± 3	8.2 ± 0.5
$C3_{net}$	2025 ± 0.5	17 ± 0.5	63 ± 3	7.6 ± 0.5
$C11_{ind}$	2024 ± 0.5	17 ± 0.5	62 ± 3	6.8 ± 0.5
$C4_{ind}$	2026 ± 0.5	18 ± 0.5	57 ± 3	6.7 ± 0.5
$C3_{ind}$	2028 ± 0.5	17 ± 0.5	67 ± 3	3.3 ± 0.5
$C11−C3_{net}(50\%)$	2026 ± 0.5	17 ± 0.5	63 ± 5	5.4 ± 0.5
$C11−C3_{net}(25\%)$	2029 ± 0.5	18 ± 0.5	58 ± 5	3.0 ± 0.5
$C11_{ind}(base-free)$	2031 ± 0.5	17 ± 0.5		1.4 ± 0.5

[a]fwhm = full width at half-maximum of the absorption band, θ = polar angle between the carbonyl symmetric stretch transition dipole and the surface normal, and Γ_{surf} = surface density of metal carbonyl headgroups.

To determine the surface density of the headgroups for the anisotropic monolayers from the absorption band area, the orientation of the mode's transition dipole is required. The carbonyl symmetric stretching mode's transition dipole has a clearly defined direction. The angle θ is the polar angle between the transition dipole vector of the carbonyl symmetric stretching mode and the surface normal of the substrate. We measured θ by polarization-resolved infrared absorption experiments (see section 2.2 and the Supporting Information). As shown in Table 1, θ is in the range of 62° ± 5° for all the samples. For the C11, C4, and C3 chains, there is no systematic difference in the orientation of the headgroups between network and independent attachment to the surface.

The surface density of headgroups, Γ_{surf} (see Table 1), was determined using the θ value and the calibration with the ICP-MS measurement. Generally, the surface density of alkyl chains

in independently attached monolayers will be lower than that of network monolayers.[72] This can be attributed to the difference in the monolayer deposition mechanism. During deposition of network monolayers, the alkyltrichlorosilanes first partially polymerize into floating monolayer patches in solution and then the networks attach to the silica substrate.[3] In contrast, the independently attached monolayers are formed by the direct reaction between surface hydroxyl groups on silica and the monochlorosilanes without polymerization. As a result, the surface density of independently attached monolayers is limited by the density of hydroxyl groups on the silica surface. By using a base-catalyzed reaction scheme, we formed independently attached monolayers which utilized the surface hydroxyl groups to the maximum extent.[58] Nonetheless, the Γ_{surf} of $C11_{ind}$ is ~80% of that of $C11_{net}$. In section 3.3 below, we show that, for chain densities >50%, the density does not significantly affect the dynamics. Therefore, in spite of some difference in surface densities, it is still appropriate to compare the results for the network and independent monolayers. However, the head-group density of $C3_{ind}$ is significantly lower than that of $C3_{net}$. This difference is likely due to less efficient substitution of Cl by azide compared to Br used in the headgroup attachment of all of the other monolayers. The reduction in headgroup density does not necessarily mean that the chain density is reduced.

The CO symmetric stretch vibrational lifetimes for the network and independently attached monolayers measured with HDTG experiments are listed in the τ_{VR} column of Table 2. The lifetimes are all ~20 ps with no systematic variation among the samples.

Table 2. Results of Dynamical Measurement for Network and Independently Attached Alkyl Monolayers[a]

sample	τ_{VR} (ps)	Γ (cm^{-1})	T_2 (ps)	Δ_1 (cm^{-1})	τ_1 (ps)
$C11_{net}$	21.6 ± 1	2.8	3.8	15.5 ± 0.5	34 ± 1
$C4_{net}$	17.7 ± 1	2.0	2.7	17.0 ± 0.5	42 ± 2
$C3_{net}$	19.5 ± 1	1.5	2.0	16.2 ± 0.5	66 ± 2
$C11_{ind}$	19.7 ± 1	2.3	3.1	15.8 ± 0.5	33 ± 1
$C4_{ind}$	20.0 ± 1	1.5	2.0	17.3 ± 0.5	42 ± 2
$C3_{ind}$	19.3 ± 1	2.7	3.7	15.6 ± 0.5	74 ± 3

[a]Because FFCF decays as a single exponential, Δ_1 is the total inhomogeneous width. The total absorption line shape is the convolution of the homogeneous Lorentzian line with width Γ and the inhomogeneous line with width Δ_1.

Figure 2 shows a series of 2D IR spectra taken at two T_w values, 0.5 and 25 ps. In the top left panel, the dashed line is the diagonal. Figure 2A shows the spectra for $C11_{net}$, and Figure 2B shows the spectra for $C11_{ind}$. At short time (0.5 ps), the spectra are substantially elongated along the diagonal. As time increases, the spectra become less elongated. As discussed in section 2.3, the dynamical information is contained in the change in shape of the spectra as T_w increases. The main bands (red, positive going) arise from the 0−1 vibrational transition. In some of the panels a portion of a blue band (negative going) below the 0−1 band can be seen. These bands are from the 1−2 transition. A full spectrum is shown in the Supporting Information). The data analysis is performed on the 0−1 band. The spectra in parts A and B are qualitatively the same, which indicates that there is no significant difference in the dynamics of the network and independently attached monolayers.

The change in shape with T_w can be quantified using the CLS method, which in turn gives the FFCF (section 2.3).[61,62]
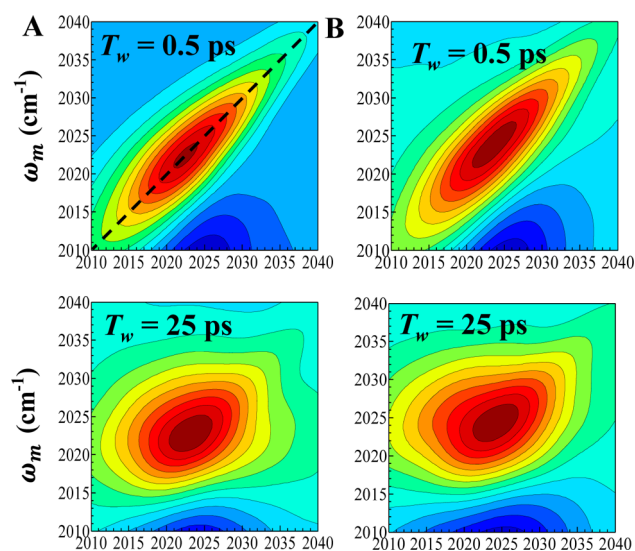

Figure 2. (A) 2D IR spectra of $C11_{net}$. (B) 2D IR spectra of $C11_{ind}$. The spectra are shown for two T_w values: 0.5 and 25 ps.
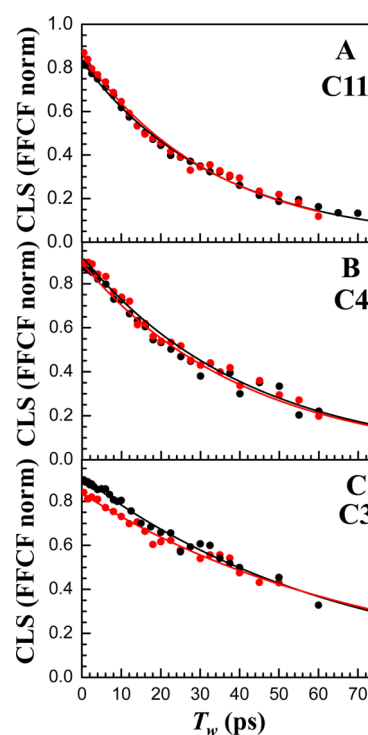

Figure 3. Center line slope decay curves (normalized FFCF) extracted from 2D IR spectra comparing network monolayers (black) vs independently attached monolayers (red) with various chain lengths: (A) $C11_{net}$ and $C11_{ind}$, (B) $C4_{net}$ and $C4_{ind}$, (C) $C3_{net}$ and $C3_{ind}$. The solid curves (black, network; red, independent) are exponential fits to the data.

Figure 3 displays CLS decay curves obtained from a series of spectra like those shown in Figure 2. In each panel, the data are for network attached (black points) and independently attached (red points) monolayers. The solid curves through the data (black, network; red, independent) are single-exponential fits. From the data and the linear absorption spectra, the FFCFs are obtained. The FFCF parameters are listed in Table 2. In parts A and B of Figure 3, for C11 and C4 chains, respectively, the network and independent monolayers

display identical dynamics as shown by the τ_1 (spectral diffusion) values in Table 2. For the C3 data and fits in Figure 3C, the network data are slightly faster than the independent data; however, the decays are almost within the error bars (see Table 2). The small difference may be attributed to the very low headgroup density of $C3_{ind}$ as discussed above.

All of the decays were fit with single exponentials without offsets (an exponential without an additive constant). An offset in the fit would indicate a much slower process that falls outside of the time window that is limited by the vibrational lifetime. The data in Figure 3A show clearly that no offset is needed. At 75 ps, the $C11_{net}$ decay is down to a value of 0.067, very close to zero and still dropping.

The inhomogeneous widths, Δ_1 in Table 2, are essentially the same for each chain length pair of network and independently attached monolayers. However, the homogeneous widths, Γ, and the corresponding homogeneous dephasing times, T_2, jump around a good deal. These values are difficult to extract without significant error because the absorption spectra are dominated by the inhomogeneous width and there is uncertainty in the absorption line width of ~1 cm^{-1}. However, looking at Figure 3, the initial CLS values, for T_w extrapolated to 0, are all ~0.85, which indicates that all of the samples have similar homogeneous line widths.

One might have anticipated that the difference in the nature of the surface functionalization, network attachment vs each chain independently attached to the surface, would make a significant difference in the monolayer structure and dynamics. Nonetheless, for the same length of the alkyl chains, C11, C4, or C3, the FT-IR results show that the orientations of the headgroup transition dipoles are the same within error for both attachment methods. The 2D IR results show that, for each chain length, the dynamics are the same independent of the surface attachment method.

In examining the structure and dynamics of the different monolayer samples, it is important to recall that the chains are first attached to the surface and then the headgroups are attached to the surface-bound chains. Thus, the bulky headgroups do not influence how the chains form the surface monolayers. The headgroup and triazole ring are rigid and only have vibrational modes that do not contribute to spectral diffusion. Vibrations, which are quantized motions, do not result in sampling different frequencies in the inhomogeneous line, which is necessary to cause spectral diffusion. Therefore, the spectral diffusion originates from the alkyl chain dynamics. Previously, it was shown that the headgroup orientation and structural dynamics of the functionalized monolayers did not depend on the surface density of the headgroups when the density of the alkyl chains remained unchanged but only a fraction of them were terminated with the headgroups.[52] This fact also indicates that the possible constraints imposed by the headgroups do not have a major influence on the comparisons of the chain dynamics.

These considerations indicate that the spectral diffusion is associated with collective and individual motions of the alkyl chains. It is important to note that the vapor-deposited SiO_2 surface is not crystalline. The independent attachment of alkyl chains (monochlorosilane precursors) does not form a uniform lattice-like packing structure like, for example, alkylthiolate monolayers on a crystalline gold surface.[5] The quasi-polymeric network formed with the alkyltrichlorosilane precursors will also not produce a lattice-like packing of chains.[3] Thus, the packed chains in network or independently attached alkylsilox-

ane monolayers have gauche defects, as demonstrated by the shift of the methylene C–H stretching frequency from the all-trans frequency (see above). The disorder of the chains will result in free volume within the monolayer structure and the ability of the structure to fluctuate among many local and more global configurations. These chain fluctuations involving motions of individual chains and groups of chains will produce spectral diffusion. The spectral diffusion dynamical data and FT-IR measurements of the headgroup transition dipole direction are experimentally indistinguishable for independent chains directly attached or a network of chains collectively attached, demonstrating that different manners of chain attachment to the silica surface yield chain packing structures and dynamics that are virtually identical.

3.2. Monolayers with Different Chain Lengths. In section 3.1 it was shown that the headgroup orientations for C11, C4, and C3 monolayers were similar, within the range of $62 \pm 5°$. For both the network and independently attached monolayers, Γ_{surf} showed a small decrease as the chain length decreased (see Table 1). We attribute the small decrease in the headgroup surface density to changes in the packing of the shorter alkyl chains. The much smaller Γ_{surf} for $C3_{ind}$ was discussed in section 3.1. As noted previously[52] and discussed further in section 3.3, small changes in the headgroup density do not influence the dynamics measured with 2D IR.

We first compare the 2D IR data for $C11_{net}$, $C4_{net}$, and $C3_{net}$. Previously it was noted that there is a significant slowing of the spectral diffusion in going from a C11 to a C3 chain.[54] Here the data have higher quality, and there are additional data for the C4 chains. Table 2 gives the spectral diffusion times, τ_1, for $C11_{net}$, $C4_{net}$, and $C3_{net}$, which are 34, 42, and 66 ps. In going from C11 to C4, a reduction of seven methylenes, the spectral diffusion slows by ~25%. However, in going from C4 to C3, a change of one methylene, the spectral diffusion slows by an additional 60%. Therefore, in going from C11 to C4, a large change in chain length only causes a relatively mild slowing of the chain dynamics, but a further reduction in chain length by one methylene makes a large difference. The data for the independently attached chains show the same trend, with the $C11_{ind}$, $C4_{ind}$, and $C3_{ind}$ samples having spectral diffusion times of 33, 42, and 74 ps, respectively (see Table 2).

These results indicate that the chain structural fluctuations are more restricted for the methylene units near the silica substrate than for the portions of the chains that are further away from the substrate surface. It has been established that the top parts of the alkyl monolayers are generally more randomly packed and have more structural freedom due to the lack of constraints,[3] which is consistent with the dynamical results obtained here. The net result is that the chain dynamics and the nature of chain packing are little changed once the chains become sufficiently long, >C3. It is informative that there is a large change in going from C4 to C3. C4 seems to be a dividing point where the upper portions of the chains that are freer to undergo fast fluctuations start to be affected by the restrictions in the lower portions of the chains. Because of the lack of starting materials, we could not examine chain lengths between C4 and C11. Chain lengths between C4 and C11 are not available with terminal-brominated alkyltrichlorosilanes or alkylmonochlorosilanes. However, the relatively small difference in the spectral diffusion time constants in going from C11 to C4 suggests that, for lengths between these two, the dynamics will be very similar.

3.3. Monolayers with Decreasing Surface Density of the C11 Chain. To study the impact of the chain density on the monolayer dynamics, a series of mixed network monolayers with different C11 chain densities were prepared. In these monolayers, a controlled fraction of C3 chains replaced the C11 chains as spacers. The C3 chains were terminated with methyl groups, and only C11 chains were functionalized with the metal carbonyl headgroups. Thus, the 2D IR experiments were observing the monolayer dynamics through the C11 chain vibrational probes. By using the C3 chains, the total alkyl chain density on the substrate is not reduced. However, for the C11 chains, above the third methylene from the surface, the chains will be less tightly packed. As shown above in section 3.2, for a fully functionalized C11 surface, a good deal of the dynamics occurs above the first three methylenes.

Mixed network monolayers were prepared with two C11 concentrations, $C11-C3_{net}(50\%)$ and $C11-C3_{net}(25\%)$, where the percentage gives the fraction of C11 trichlorosilanes among all the trichlorosilanes in solution during the monolayer deposition. Mixed monolayers are free from phase segregation of the different chain lengths as long as the ratio of the number of the two types of chains is not extreme.[73,74] The homogeneity of mixed monolayers was verified by FT-IR spectra discussed below. Attempts to prepare $C11-C3_{net}(10\%)$ were not reproducible, and the monolayers formed were inhomogeneous. To prepare a monolayer with C11 chains less than 25% of full density, a different type of sample was made. Direct attachment of independent chains using monochlorosilane as the precursor but without adding the base catalyst generated C11 monolayers with ~15% of the chain density of the $C11_{net}$ monolayers. These samples are called $C11_{ind}$(base-free). Schematic illustrations of the $C11-C3_{net}(50\%)$ and the $C11_{ind}$(base-free) are shown in Figure 1D,E.

Figure 4A displays the C–H stretching region of the FT-IR spectra of monolayers with different C11 chain densities. The pink line is the spectrum of a SiO_2/CaF_2 wafer without monolayer deposition, showing that absorption caused by adventitiously adsorbed organic materials was very small. From $C11_{net}$ to $C11_{ind}$(base-free), as the long C11 chain density was decreased, the absorbance of the methylene peaks was reduced. The antisymmetric and symmetric stretching modes of methyl groups at 2873 and 2962 cm^{-1} for $C11-C3_{net}(50\%)$ and $C11-C3_{net}(25\%)$ monolayers are apparent. These peaks are attributed to the methyl-terminated C3 chains.

Figure 4B displays the carbonyl symmetric stretch region of the FT-IR spectrum. The reduction of the C11 chain density has two effects on the spectrum. First, because the headgroups in this series of monolayers were only attached to the C11 chains, the peak area decreased as the C11 chain density decreased. Second, the peak position shifted to the blue as the headgroup coverage was reduced. The vibrational frequency of the headgroup is sensitive to its chemical environments.[53] There was no change in chemical composition of the samples except for the surface concentration of the headgroups. The change in the headgroup frequency shows that the interactions of the headgroups with their environments change with the chain density. One possibility is that the headgroups interact differently with the alkyl portions of the surrounding chains as the C11 density goes down. Another possibility is a shift of the vibrational frequency caused by the vibrational Stark effect.[75,76] The headgroups have a significant dipole moment. Each headgroup will experience an electric field that is the vector sum of the fields originating from the other headgroups as well
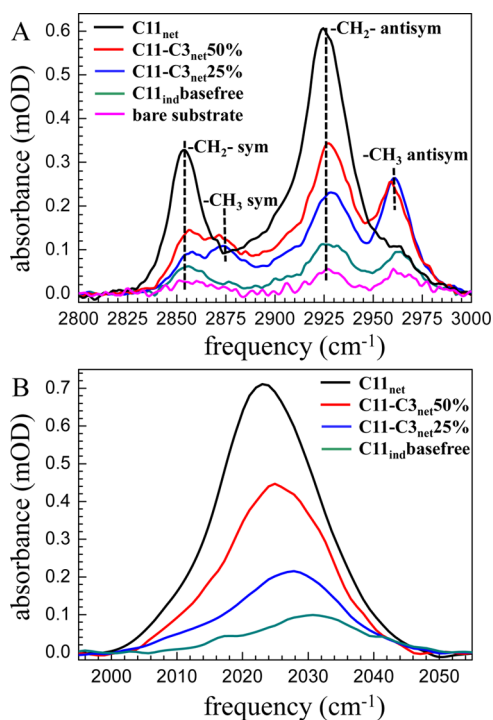

Figure 4. Unpolarized infrared absorption spectra. (A) C–H stretching region of $C11_{net}$ (black), $C11-C3_{net}(50\%)$ (red), $C11-C3_{net}(25\%)$ (blue), $C11_{ind}$(base-free) (green), and background substrate (pink). (B) Symmetric carbonyl stretching region of the headgroup vibrational probe. The colors are for the same samples as in (A).

as from the alkyl chains. As the headgroup density decreases, the resulting electric field at a particular headgroup will, on average, decrease, reducing the Stark effect contribution to the vibrational frequency, producing a frequency shift. The center frequencies of the various samples are given in Table 1. The gradual shift of the frequency with the headgroup density also supports the studies that show mixtures of chain lengths do not segregate.[73,74] If the C11 chains in the C11–C3 mixtures (no headgroups on the C3 chains) form C11 clusters, there would be no or little change in the Stark effect or other changed intermolecular interactions and no frequency shift. Similar spectral shifts caused by the Stark effect have been described for the infrared spectra of vibrations immersed in different solvents.[77] As discussed further below, the Stark effect can also be the coupling mechanism that produces spectral diffusion from the alkyl chain motions. As the monolayer structure fluctuates, time-dependent electric fields will be produced that can cause spectral diffusion.[64,78−80]

Although the chain density varied, θ was still in the range of 62° ± 5°. However, the 58° angle for the $C11-C3_{net}(25\%)$ monolayers could be caused by a change in the distribution of angles. The angle obtained from the polarized FT-IR measurements is actually determined by both the tilt angle of the transition dipoles relative to the surface normal and the cone of angles around the average tilt angle. For moderately narrow cones, the angle is basically the tilt angle. However, as the cone angle becomes wide, the measurement does not uniquely determine the tilt angle.[81] It is reasonable to propose that a significant reduction of the C11 chain density leads to a greater distribution of the individual chain structures, resulting in a broader cone of angles with possibly a different average

value, which will alter the value of θ. The θ values are given in Table 1. The value for the C11$_{ind}$(base-free) monolayer is not listed, because its absorbance was too low to conduct a reliable polarization-resolved measurement.

The Γ_{surf} value for C11−C3$_{net}$(50%) is slightly higher than half of the value for C11$_{net}$. This is due to the fact that every azide group on the C11 chains of C11−C3$_{net}$(50%) monolayers was consumed during functionalization, which is not the case for C11$_{net}$ monolayers because of excluded area caused by the large size of the headgroup.[52,74] The Γ_{surf} value for C11−C3$_{net}$(25%) is very close to half of the value for C11−C3$_{net}$(50%). The trend in the surface density of the headgroups supports that the mixed monolayers of the C3 and C11 chains control the C11 chain density as designed without clustering of the C11 chains. The θ value of C11−C3$_{net}$(25%) was used when the headgroup surface density for C11$_{ind}$(base-free) was calculated. The Γ_{surf} value for this monolayer is about half of that for C11−C3$_{net}$(25%).

The plots of the CLS decays for the four samples, C11$_{net}$ (black), C11−C3$_{net}$(50%) (red), C11−C3$_{net}$(25%) (blue), and C11$_{ind}$(base-free) (green), are shown in Figure 5. (The C11$_{net}$
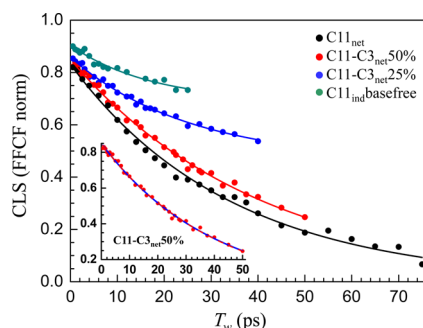

Figure 5. Center line slope decay curves (normalized FFCF) extracted from 2D IR spectra of monolayers with various C11 chain densities: C11$_{net}$ (black points), C11−C3$_{net}$(50%) (red points), C11−C3$_{net}$(25%) (blue points), C11$_{ind}$(base-free) (green points). The solid curves are fits to the data. The inset shows the C11−C3$_{net}$(50%) (red points) data and two fits: red dashed curve, single-exponential fit; blue dashed curve, biexponential fit.

curve is the same as the one in Figure 3A.) The FFCF parameters are given in Table 3. As the concentration of C11 chains, and therefore the concentration of the vibrational probe headgroups, is reduced, the signal is also reduced, which limits the time range over which data can be collected. While the decay of the C11−C3$_{net}$(50%) (red) sample is similar to that of the C11$_{net}$ (black) sample, the lower C11 concentration samples are fundamentally different. (The C11−C3$_{net}$(50%) curve is discussed further below.) For the C11−C3$_{net}$(25%)

(blue) and C11$_{ind}$(base-free) (green) samples, CLS decays cannot be fit reasonably as a single-exponential decay to zero. Rather, they are fit as an exponential decay to an offset (a horizontal nonzero baseline). The amplitude of the offset shows that this component comprises more than half of the total inhomogeneous line width. An offset reflects a very slow component with a decay constant that cannot be measured given the limited time window of the experiments. In Table 3 for these samples, τ_1 is the spectral diffusion time constant and Δ_1 is its associated frequency fluctuation amplitude (width in the absorption line). Δ_2 is the amplitude of the offset. There is no corresponding τ_2 because it is too slow to measure. Δ_{inh} in Table 3 is the total inhomogeneous contribution to the absorption line. It is the convolution of the two Gaussian inhomogeneous components.

For the samples with the two lowest chain densities, C11−C3$_{net}$(25%) and C11$_{ind}$(base-free) (∼15%), as the chain density is reduced, the fast spectral diffusion component becomes increasingly fast, 25 and 17 ps, respectively (see Table 3), which are faster than that of the pure C11 monolayer, C11$_{net}$. The amplitude of the very slow spectral diffusion (offset term), Δ_2, is larger and the amplitude of the fast dynamics, Δ_1, is smaller for C11$_{ind}$(base-free) than for C11−C3$_{net}$(25%) (see Table 3). Thus, as the C11 chain density is reduced, there is a shift in amplitude from fast spectral diffusion to very slow spectral diffusion. In addition, the two low-coverage samples have a wider inhomogeneous width, Δ_{inh}, than the pure C11 monolayer. The wider inhomogeneous width indicates that there are more structural environments that influence the vibrational frequency.

The offset terms in CLS decay curves for the two low-coverage samples show that there are structural microstates that are very slow to randomize. It is also possible that they will not randomize on any reasonable time scale. The offset term in the FFCF, Δ_2, is likely caused by highly disordered packing of the alkyl chains. At low chain density, the long C11 chains are not sterically supported by the surrounding chains in a nearly upright configuration relative to the surface, and may tend to bend over and form nonlinear "collapsed" structures. Measurements of the thickness of the monolayers via ellipsometry identified the formation of collapsed structures far from linear in alkylsiloxane monolayers with very low chain density.[82] The collapsed structures may result in entangled chains that have very high barriers for structural randomization that gives rise to complete spectral diffusion. The collapsed and loosely packed structure can give rise to some fast structural evolution that samples a fraction of the inhomogeneously broadened absorption line, but entanglement results in a portion of the structures that can only be sampled on very long time scales.

Table 3. Dynamical Parameters as a Function of the Monolayer Chain Density[a]

sample	τ_{VR} (ps)	Γ (cm^{-1})	T_2 (ps)	Δ_1 (cm^{-1})	τ_1 (ps)	Δ_2[b] (cm^{-1})	Δ_{inh} (cm^{-1})
C11$_{net}$	21.6 ± 1	2.8	3.8	15.5	34 ± 1		15.5
C11−C3$_{net}$(50%)	21.6 ± 1	2.5	3.4	15.7	40 ± 1		15.7
C11−C3$_{net}$(25%)	21.2 ± 1	2.6	3.5	11.4	25 ± 2	12.2	16.7
C11$_{ind}$(base-free)	15.7 ± 1	1.5	2.0	8.0	17 ± 5	14.1	16.2

[a]The total absorption line shape is the convolution of the homogeneous Lorentzian line with width Γ and the total inhomogeneous line with width Δ_{inh}. For the first two rows, the FFCF has only the homogeneous dephasing and a single component of spectral diffusion. Then $\Delta_1 = \Delta_{inh}$. For the last two rows, the FFCF has two contributions to the inhomogeneous component, Δ_1 and Δ_2. The total inhomogeneous line width is $\Delta_{inh} = (\Delta_1{}^2 + \Delta_2{}^2)^{1/2}$. [b]Offset, τ_2 too long to measure within the experimental time window determined by the vibration lifetime.

Returning to the C11−C3$_{net}$(50%) sample, the data are fit with a single exponential, in contrast to the lower density samples. However, the decay time constant, 40 ps, is somewhat slower than the 34 ps decay time constant of the samples with full C11 coverage, C11$_{net}$. One possibility is that the C11−C3$_{net}$(50%) samples do develop faster and slower components to the CLS decay, but the change is too small to observe. The inset in Figure 5 shows the C11−C3$_{net}$(50%) data (red points) and two fits. The red dashed curve is the single-exponential decay that yields 40 ps as in the main portion of the sample. The blue dashed curve is a biexponential fit with time constants of 30 and 45 ps, where one time constant was fixed at 30 ps and the other allowed to float. This curve is indistinguishable from the single-exponential fit. This fit has a component that is faster than the fit to the C11$_{net}$ data and a component that is slower, like the lower density samples, but unlike the lower density samples, the slow and fast components are not different enough to resolve. If the fast component is fixed at a value much below 30 ps, the fit yields its amplitude as essentially zero, and returns ∼40 ps for the other decay, which is basically the single-exponential fit to the data. The net result is that reduction from full coverage to 50% coverage does not have a large effect on the dynamics. Only when the chain density becomes even lower are obvious changes in the dynamics and inhomogeneous line widths observed.

4. CONCLUDING REMARKS

We have investigated a series of functionalized alkylsiloxane monolayers by infrared linear absorption spectroscopy and nonlinear time-resolved 2D IR spectroscopy. The infrared linear absorption spectroscopy combined with ICP-MS verified that the monolayer samples had good quality and high surface density. The rhenium carbonyl headgroup, which mimics the headgroups found in many applications, served as the vibrational probe for investigating the fast structural dynamics of the monolayers using 2D IR to measure spectral diffusion.

Spectral diffusion is produced by the structural evolution of a system that causes vibrational chromophores to sample different frequencies within the inhomogeneously broadened absorption spectrum because the frequency is coupled to the structure. A coupling mechanism has been used in MD simulations to successfully reproduce the experimental data of systems such as proteins, water, and room temperature ionic liquids is the vibrational Stark effect.[63,64,78−80,83] As the structure of a system evolves in time, the electric field produced by all of the constituents of the system projected onto the vibrational transition dipole fluctuates because of the changing positions of the various moieties. These electric field fluctuations cause the vibrational frequency to fluctuate through the Stark effect. In a simulation, the partial charges on all of the components of the system produce a resultant time-dependent electric field along the vibration's transition dipole. The time-dependent electric field produces the frequency fluctuations that are measured in a 2D IR experiment as spectral diffusion. This method has been remarkably successful in reproducing the FFCF of complex systems.[63,64,79,80,83] The time dependence is independent of the value of the Stark coupling constant, which can be adjusted to reproduce the absorption spectrum line width. In a number of cases where the Stark coupling constant is known from experiments, the simulations have resulted in Stark constants that are consistent with the independently measured values, which supports the validity of the Stark mechanism for spectral diffusion.[64,83]

Preliminary simulations of C11 chains with the RePhen-(CO)$_3$Cl headgroup and triazole ring on crystalline SiO$_2$ have been performed.[84] The fluctuating electric field with Stark coupling model was used, and the preliminary FFCF is reasonable but somewhat slower than the experimental results for the amorphous silica substrate. While these preliminary results cannot be directly compared to the experimental results on amorphous SiO$_2$, they do provide insights into the nature of the dynamics. The headgroups reside at the top of the monolayer. Chains do not bend over and bury the headgroups in the alkyl region of the monolayer. The decay of the FFCF is produced by motions of the alkyl chains. These motions cause the headgroups to move. There are frequent partial rotations of the methylenes as well as gauche−trans isomerizations, and concerted isomerizations of several methylene groups along the alkyl chains. These motions cause the headgroups to move up and down to some extent and produce some angular fluctuations of the headgroups but do not necessarily result in large changes in the headgroup orientation. The entire chains bend back and forth from motions at the points of attachment to the SiO$_2$ crystal. 2D IR experiments on crystalline gold will be compared quantitatively to simulations on crystalline gold, which are in progress.[84] In addition to simulating the FFCF, various single-chain orientation and position correlation functions as well as collective correlation functions will be calculated. These simulations will provide a detailed understanding of the chain motions that are responsible for the decay of the FFCF.

In the results presented above, two methods of forming alkylsiloxane monolayers on SiO$_2$ surfaces were studied. One method used monochlorosilane with the assistance of a base catalyst to form monolayers where independent chains are directly attached to the silica surface. The other method used trichlorosilane as the precursor where trichlorosilanes react in solution to form networks of interlinked chains. The chain networks then attach to the surface. Polarized FT-IR absorption experiments showed that the manner of attachment did not change the direction of the IR transition dipole of the CO stretching mode of the metal carbonyl headgroup. The lack of a change of the transition dipole directions indicates that the method of attachment does not have a significant impact on the structure of monolayers above the silica surface. The 2D IR experiments showed that the chain dynamics were independent of the manner of attachment for several alkyl chain lengths.

The influence of the alkyl chain lengths on the monolayer dynamics was also investigated for three chain lengths, C11, C4, and C3, for both methods of attachment. The same trend was observed with either manner of attachment. In going from C11 to C4, a reduction of seven methylene moieties, the dynamics slowed mildly, from 34 to 42 ps. However, the reduction of the chain length by one more methylene to C3 slowed the dynamics to ∼70 ps. These results indicate that motions of the chains near the substrate are significantly slower than those further away, and that the chain structural fluctuations are not greatly sensitive to the chain length once the chain is sufficiently long.

Finally, the influence of the chain density on the monolayer structural dynamics was investigated for a series of monolayers with decreasing C11 chain density. Two samples were prepared with lower C11 chain density, 50% C11 and 25% C11, by cofunctionalizing the surface with C11 and C3 chains. Only the C11 chains had the vibrational probe. Another sample was prepared with an even lower surface density of C11 chains,

~15% of that of the fully packed monolayers, by using the monochlorosilane precursor without the assistance of the base catalyst. Going from 100% C11 to 50% C11 had only a minor effect on the monolayer structural dynamics. However, for 25% and 15%, there was a fundamental change in the nature of the dynamics. While the 100% samples displayed spectral diffusion with single-exponential time dependence, the 25% and 15% samples yielded spectral diffusion with two components, one that is faster than the 100% C11 monolayer dynamics and one that is very slow, too slow to measure in the experimental time window determined by the vibrational lifetime. It was suggested that the change in dynamics is caused by collapsed chain structures that are very different from those of high-chain-density samples. The collapsed structures can still have fast structural dynamics that sample a fraction of the inhomogeneously broadened absorption line, but a large portion of the collapsed structures have high barriers for structural randomization that occurs on long time scales.

The experiments reported here were made possible by applicability of 2D IR spectroscopy to monolayers. They have provided information on the relationship between the monolayer structure and dynamics for alkylsiloxane monolayers on a SiO_2 surface.

■ ASSOCIATED CONTENT

Ⓢ Supporting Information

Descriptions of the preparation of monolayer samples, procedures of the ICP-MS measurements, details of extracting the polar angle of the transition dipole, θ, of the carbonyl symmetric stretching mode, and a 2D IR spectrum showing both 0−1 and 1−2 bands of the headgroup are included. The Supporting Information is available free of charge on the ACS Publications website at DOI: 10.1021/acs.jpcc.5b05641.

■ AUTHOR INFORMATION

Corresponding Author
*E-mail: fayer@stanford.edu.

Notes
The authors declare no competing financial interest.

■ ACKNOWLEDGMENTS

■ REFERENCES

(1) Miro, P.; Audiffred, M.; Heine, T. An Atlas of Two-Dimensional Materials. *Chem. Soc. Rev.* **2014**, *43*, 6537−6554.

(2) Kissel, P.; Murray, D. J.; Wulftange, W. J.; Catalano, V. J.; King, B. T. A Nanoporous Two-Dimensional Polymer by Single-Crystal-to-Single-Crystal Photopolymerization. *Nat. Chem.* **2014**, *6*, 774−778.

(3) Ulman, A. Formation and Structure of Self-Assembled Monolayers. *Chem. Rev.* **1996**, *96*, 1533−1554.

(4) Maoz, R.; Sagiv, J. On the Formation and Structure of Self-Assembling Monolayers. I. A Comparative ATR-Wettability Study of Langmuir−Blodgett and Adsorbed Films on Flat Substrates and Glass Microbeads. *J. Colloid Interface Sci.* **1984**, *100*, 465−496.

(5) Love, J. C.; Estroff, L. A.; Kriebel, J. K.; Nuzzo, R. G.; Whitesides, G. M. Self-Assembled Monolayers of Thiolates on Metals as a Form of Nanotechnology. *Chem. Rev.* **2005**, *105*, 1103−1169.

(6) Sagiv, J. Organized Monolayers by Adsorption. 1. Formation and Structure of Oleophobic Mixed Monolayers on Solid-Surfaces. *J. Am. Chem. Soc.* **1980**, *102*, 92−98.

(7) Haensch, C.; Hoeppener, S.; Schubert, U. S. Chemical Modification of Self-Assembled Silane Based Monolayers by Surface Reactions. *Chem. Soc. Rev.* **2010**, *39*, 2323−2334.

(8) Hsieh, S. C.; Chao, W. J.; Lin, P. Y.; Hsieh, C. W. Influence of Molecular Packing on the Corrosion Inhibition Properties of Self-Assembled Octadecyltrichlorosilane Monolayers on Silicon. *Corros. Sci.* **2014**, *80*, 427−433.

(9) Song, Y.; Nair, R. P.; Zou, M.; Wang, Y. Q. Superhydrophobic Surfaces Produced by Applying a Self-Assembled Monolayer to Silicon Micro/Nano-Textured Surfaces. *Nano Res.* **2009**, *2*, 143−150.

(10) Onclin, S.; Mulder, A.; Huskens, J.; Ravoo, B. J.; Reinhoudt, D. N. Molecular Printboards: Monolayers of β-Cyclodextrins on Silicon Oxide Surfaces. *Langmuir* **2004**, *20*, 5460−5466.

(11) Turgeman, R.; Gershevitz, O.; Palchik, O.; Deutsch, M.; Ocko, B. M.; Gedanken, A.; Sukenik, C. N. Oriented Growth of Zno Crystals on Self-Assembled Monolayers of Functionalized Alkyl Silanes. *Cryst. Growth Des.* **2004**, *4*, 169−175.

(12) Taguchi, T.; Isozaki, K.; Miki, K. Enhanced Catalytic Activity of Self-Assembled-Monolayer-Capped Gold Nanoparticles. *Adv. Mater.* **2012**, *24*, 6462−6467.

(13) Liu, D.; Lie, Y.; Shao, H.; Jiang, X. Using Azobenzene-Embedded Self-Assembled Monolayers To Photochemically Control Cell Adhesion Reversibly. *Angew. Chem., Int. Ed.* **2009**, *48*, 4406−4408.

(14) Turchanin, A.; Tinazli, A.; El-Desawy, M.; Großmann, H.; Schnietz, M.; Solak, H. H.; Tampé, R.; Gölzhäuser, A. Molecular Self-Assembly, Chemical Lithography, and Biochemical Tweezers: A Path for the Fabrication of Functional Nanometer-Scale Protein Arrays. *Adv. Mater.* **2008**, *20*, 471−477.

(15) Ma, H.; Acton, O.; Hutchins, D. O.; Cernetic, N.; Jen, A. K.-Y. Multifunctional Phosphonic Acid Self-Assembled Monolayers on Metal Oxides as Dielectrics, Interface Modification Layers and Semiconductors for Low-Voltage High-Performance Organic Field-Effect Transistors. *Phys. Chem. Chem. Phys.* **2012**, *14*, 14110−14126.

(16) Allara, D. L.; Parikh, A. N.; Rondelez, F. Evidence for a Unique Chain Organization in Long-Chain Silane Monolayers Deposited on Two Widely Different Solid Substrates. *Langmuir* **1995**, *11*, 2357−2360.

(17) Tripp, C. P.; Hair, M. L. An Infrared Study of the Reaction of Octadecyltrichlorosilane with Silica. *Langmuir* **1992**, *8*, 1120−1126.

(18) Liu, Y.; Wolf, L. K.; Messmer, M. C. A Study of Alkyl Chain Conformational Changes in Self-Assembled *n*-Octadecyltrichlorosilane Monolayers on Fused Silica Surfaces. *Langmuir* **2001**, *17*, 4329−4335.

(19) Lagutchev, A. S.; Song, K. J.; Huang, J. Y.; Yang, P. K.; Chuang, T. J. Self-Assembly of Alkylsiloxane Monolayers on Fused Silica Studied by XPS and Sum Frequency Generation Spectroscopy. *Chem. Phys.* **1998**, *226*, 337−349.

(20) Vallant, T.; Brunner, H.; Mayer, U.; Hoffmann, H.; Leitner, T.; Resch, R.; Friedbacher, G. Formation of Self-Assembled Octadecylsiloxane Monolayers on Mica and Silicon Surfaces Studied by Atomic Force Microscopy and Infrared Spectroscopy. *J. Phys. Chem. B* **1998**, *102*, 7190−7197.

(21) Wang, H. F.; Gan, W.; Lu, R.; Rao, Y.; Wu, B. H. Quantitative Spectral and Orientational Analysis in Surface Sum Frequency Generation Vibrational Spectroscopy (SFG-VS). *Int. Rev. Phys. Chem.* **2005**, *24*, 191−256.

(22) Richmond, G. L. Molecular Bonding and Interactions at Aqueous Surfaces as Probed by Vibrational Sum Frequency Spectroscopy. *Chem. Rev.* **2002**, *102*, 2693−2724.

(23) Eisenthal, K. B. Liquid Interfaces Probed by Second-Harmonic and Sum-Frequency Spectroscopy. *Chem. Rev.* **1996**, *96*, 1343−1360.

(24) Gengeliczki, Z.; Rosenfeld, D. E.; Fayer, M. D. Theory of Interfacial Orientational Relaxation Spectroscopic Observables. *J. Chem. Phys.* **2010**, *132*, 244703.

(25) Zhang, Z.; Piatkowski, L.; Bakker, H. J.; Bonn, M. Ultrafast Vibrational Energy Transfer at the Water/Air Interface Revealed by Two-Dimensional Surface Vibrational Spectroscopy. *Nat. Chem.* **2011**, *3*, 888−893.

(26) Inoue, K.-i.; Nihonyanagi, S.; Singh, P. C.; Yamaguchi, S.; Tahara, T. 2D Heterodyne-Detected Sum Frequency Generation Study on the Ultrafast Vibrational Dynamics of H$_2$O and HOD Water at Charged Interfaces Dynamics of H$_2$O and HOD Water at Charged Interfaces. *J. Chem. Phys.* **2015**, *142*, 212431.

(27) Xiong, W.; Laaser, J. E.; Mehlenbacher, R. D.; Zanni, M. T. Adding a Dimension to the Infrared Spectra of Interfaces Using Heterodyne Detected 2D Sum-Frequency Generation (HD 2D SFG) Spectroscopy. *Proc. Natl. Acad. Sci. U.S.A.* **2011**, *108*, 20902−20907.

(28) Laaser, J. E.; Skoff, D. R.; Ho, J. J.; Joo, Y.; Serrano, A. L.; Steinkruger, J. D.; Gopalan, P.; Gellman, S. H.; Zanni, M. T. Two-Dimensional Sum-Frequency Generation Reveals Structure and Dynamics of a Surface-Bound Peptide. *J. Am. Chem. Soc.* **2014**, *136*, 956−962.

(29) Patterson, J. E.; Lagutchev, A.; Huang, W.; Dlott, D. D. Ultrafast Dynamics of Shock Compression of Molecular Monolayers. *Phys. Rev. Lett.* **2005**, *94*, 015501.

(30) Bredenbeck, J.; Ghosh, A.; Nienhuys, H. K.; Bonn, M. Interface-Specific Ultrafast Two-Dimensional Vibrational Spectroscopy. *Acc. Chem. Res.* **2009**, *42*, 1332−1342.

(31) Bordenyuk, A. N.; Jayathilake, H.; Benderskii, A. V. Coherent Vibrational Quantum Beats as a Probe of Langmuir−Blodgett Monolayers. *J. Phys. Chem. B* **2005**, *109*, 15941−15949.

(32) Nihonyanagi, S.; Eftekhari-Bafrooei, A.; Borguet, E. Ultrafast Vibrational Dynamics and Spectroscopy of a Siloxane Self-Assembled Monolayer. *J. Chem. Phys.* **2011**, *134*, 084701.

(33) Malyk, S.; Shalhout, F. Y.; O'Leary, L. E.; Lewis, N. S.; Benderskii, A. V. Vibrational Sum Frequency Spectroscopic Investigation of the Azimuthal Anisotropy and Rotational Dynamics of Methyl-Terminated Silicon(111) Surfaces. *J. Phys. Chem. C* **2013**, *117*, 935−944.

(34) Karpovich, D. S.; Blanchard, G. J. Dynamics of a Tethered Chromophore Imbedded in a Self-Assembled Monolayer. *Langmuir* **1996**, *12*, 5522−5524.

(35) Hautman, J.; Klein, M. L. Simulation of a Monolayer of Alkyl Thiol Chains. *J. Chem. Phys.* **1989**, *91*, 4994−5001.

(36) Hautman, J.; Klein, M. L. Molecular-Dynamics Simulation of the Effects of Temperature on a Dense Monolayer of Long-Chain Molecules. *J. Chem. Phys.* **1990**, *93*, 7483−7492.

(37) Mar, W.; Klein, M. L. Molecular-Dynamics Study of the Self-Assembled Monolayer Composed of S(CH$_2$)$_{14}$CH$_3$ Molecules Using an All-Atoms Model. *Langmuir* **1994**, *10*, 188−196.

(38) Cho, M. H. Coherent Two-Dimensional Optical Spectroscopy. *Chem. Rev.* **2008**, *108*, 1331−1418.

(39) Fayer, M. D. Dynamics of Liquids, Molecules, and Proteins Measured with Ultrafast 2D IR Vibrational Echo Chemical Exchange Spectroscopy. *Annu. Rev. Phys. Chem.* **2009**, *60*, 21−38.

(40) Zheng, J. R.; Kwak, K.; Asbury, J.; Chen, X.; Piletic, I. R.; Fayer, M. D. Ultrafast Dynamics of Solute-Solvent Complexation Observed at Thermal Equilibrium in Real Time. *Science* **2005**, *309*, 1338−1343.

(41) Li, D.; Fedeles, B. I.; Singh, V.; Peng, C. S.; Silvestre, K. J.; Simi, A. K.; Simpson, J. H.; Tokmakoff, A.; Essigmann, J. M. Tautomerism Provides a Molecular Explanation for the Mutagenic Properties of the Anti-HIV Nucleoside 5-Aza-5,6-dihydro-2′-deoxycytidine. *Proc. Natl. Acad. Sci. U.S.A.* **2014**, *111*, 3252−3259.

(42) King, J. T.; Arthur, E. J.; Brooks, C. L., III; Kubarych, K. J. Crowding Induced Collective Hydration of Biological Macromolecules over Extended Distances. *J. Am. Chem. Soc.* **2014**, *136*, 188−194.

(43) Cahoon, J. F.; Sawyer, K. R.; Schlegel, J. P.; Harris, C. B. Determining Transition-State Geometries in Liquids Using 2D-IR. *Science* **2008**, *319*, 1820−1823.

(44) Kiefer, L. M.; King, J. T.; Kubarych, K. J. Dynamics of Rhenium Photocatalysts Revealed through Ultrafast Multidimensional Spectroscopy. *Acc. Chem. Res.* **2015**, *48*, 1123−1130.

(45) Perakis, F.; Widmer, S.; Hamm, P. Two-Dimensional Infrared Spectroscopy of Isotope-Diluted Ice Ih. *J. Chem. Phys.* **2011**, *134*, 204505.

(46) Shim, S. H.; Gupta, R.; Ling, Y. L.; Strasfeld, D. B.; Raleigh, D. P.; Zanni, M. T. Two-Dimensional IR Spectroscopy and Isotope Labeling Defines the Pathway of Amyloid Formation with Residue-Specific Resolution. *Proc. Natl. Acad. Sci. U.S.A.* **2009**, *106*, 6614−6619.

(47) Remorino, A.; Korendovych, I. V.; Wu, Y.; DeGrado, W. F.; Hochstrasser, R. M. Residue-Specific Vibrational Echoes Yield 3D Structures of a Transmembrane Helix Dimer. *Science* **2011**, *332*, 1206−1209.

(48) Asbury, J. B.; Steinel, T.; Stromberg, C.; Corcelli, S. A.; Lawrence, C. P.; Skinner, J. L.; Fayer, M. D. Water Dynamics: Vibrational Echo Correlation Spectroscopy and Comparison to Molecular Dynamics Simulations. *J. Phys. Chem. A* **2004**, *108*, 1107−1119.

(49) Ramasesha, K.; De Marco, L.; Mandal, A.; Tokmakoff, A. Water Vibrations Have Strongly Mixed Intra- and Intermolecular Character. *Nat. Chem.* **2013**, *5*, 935−940.

(50) Piletic, I. R.; Tan, H.-S.; Fayer, M. D. Dynamics of Nanoscopic Water: Vibrational Echo and Infrared Pump−Probe Studies of Reverse Micelles. *J. Phys. Chem. B* **2005**, *109*, 21273−21284.

(51) Rosenfeld, D. E.; Gengeliczki, Z.; Smith, B. J.; Stack, T. D. P.; Fayer, M. D. Structural Dynamics of a Catalytic Monolayer Probed by Ultrafast 2D IR Vibrational Echoes. *Science* **2011**, *334*, 634−639.

(52) Rosenfeld, D. E.; Nishida, J.; Yan, C.; Gengeliczki, Z.; Smith, B. J.; Fayer, M. D. Dynamics of Functionalized Surface Molecular Monolayers Studied with Ultrafast Infrared Vibrational Spectroscopy. *J. Phys. Chem. C* **2012**, *116*, 23428−23440.

(53) Rosenfeld, D. E.; Nishida, J.; Yan, C.; Kumar, S. K. K.; Tamimi, A.; Fayer, M. D. Structural Dynamics at Monolayer-Liquid Interfaces Probed by 2D IR Spectroscopy. *J. Phys. Chem. C* **2013**, *117*, 1409−1420.

(54) Nishida, J.; Yan, C.; Fayer, M. D. Dynamics of Molecular Monolayers with Different Chain Lengths in Air and Solvents Probed by Ultrafast 2D IR Spectroscopy. *J. Phys. Chem. C* **2014**, *118*, 523−532.

(55) Kraack, J. P.; Lotti, D.; Hamm, P. 2D Attenuated Total Reflectance Infrared Spectroscopy Reveals Ultrafast Vibrational Dynamics of Organic Monolayers at Metal-Liquid Interfaces. *J. Chem. Phys.* **2015**, *142*, 212413.

(56) Wasserman, S. R.; Tao, Y. T.; Whitesides, G. M. Structure and Reactivity of Alkylsiloxane Monolayers Formed by Reaction of Alkyltrichlorosilanes on Silicon Substrates. *Langmuir* **1989**, *5*, 1074−1087.

(57) Haensch, C.; Hoeppener, S.; Schubert, U. S. Chemical Surface Reactions by Click Chemistry: Coumarin Dye Modification of 11-Bromoundecyltrichlorosilane Monolayers. *Nanotechnology* **2008**, *19*, 035703.

(58) Fadeev, A. Y.; McCarthy, T. J. Trialkylsilane Monolayers Covalently Attached to Silicon Surfaces: Wettability Studies Indicating That Molecular Topography Contributes to Contact Angle Hysteresis. *Langmuir* **1999**, *15*, 3759−3766.

(59) Meldal, M.; Tornoe, C. W. Cu-Catalyzed Azide−Alkyne Cycloaddition. *Chem. Rev.* **2008**, *108*, 2952−3015.

(60) Park, S.; Kwak, K.; Fayer, M. D. Ultrafast 2D-IR Vibrational Echo Spectroscopy: A Probe of Molecular Dynamics. *Laser Phys. Lett.* **2007**, *4*, 704−718.

(61) Kwak, K.; Park, S.; Finkelstein, I. J.; Fayer, M. D. Frequency-Frequency Correlation Functions and Apodization in Two-Dimensional Infrared Vibrational Echo Spectroscopy: A New Approach. *J. Chem. Phys.* **2007**, *127*, 124503.

(62) Kwak, K.; Rosenfeld, D. E.; Fayer, M. D. Taking Apart the Two-Dimensional Infrared Vibrational Echo Spectra: More Information and Elimination of Distortions. *J. Chem. Phys.* **2008**, *128*, 204505.

(63) Terranova, Z. L.; Corcelli, S. A. Molecular Dynamics Investigation of the Vibrational Spectroscopy of Isolated Water in an Ionic Liquid. *J. Phys. Chem. B* **2014**, *118*, 8264−8272.

(64) Bagchi, S.; Boxer, S. G.; Fayer, M. D. Ribonuclease S Dynamics Measured Using a Nitrile Label with 2D IR Vibrational Echo Spectroscopy. *J. Phys. Chem. B* **2012**, *116*, 4034−4042.

(65) Dunbar, J. A.; Arthur, E. J.; White, A. M.; Kubarych, K. J. Ultrafast 2D-IR and Simulation Investigations of Preferential Solvation and Cosolvent Exchange Dynamics. *J. Phys. Chem. B* **2015**, *119*, 6271−6279.

(66) Smith, A. W.; Lessing, J.; Ganim, Z.; Peng, C. S.; Tokmakoff, A.; Roy, S.; Jansen, T. L. C.; Knoester, J. Melting of a *β*-Hairpin Peptide Using Isotope-Edited 2D IR Spectroscopy and Simulations. *J. Phys. Chem. B* **2010**, *114*, 10913−10924.

(67) Fayer, M. D. Dynamics of Molecules in Condensed Phases: Picosecond Holographic Grating Experiments. *Annu. Rev. Phys. Chem.* **1982**, *33*, 63−87.

(68) Deeg, F. W.; Fayer, M. D. Analysis of Complex Molecular Dynamics in an Organic Liquid by Polarization Selective Subpicosecond Transient Grating Experiments. *J. Chem. Phys.* **1989**, *91*, 2269−2279.

(69) Fourkas, J. T.; Fayer, M. D. The Transient Grating: A Holographic Window to Dynamic Processes. *Acc. Chem. Res.* **1992**, *25*, 227−233.

(70) Snyder, R. G.; Strauss, H. L.; Elliger, C. A. C−H Stretching Modes and the Structure of *n*-Alkyl Chains. 1. Long, Disordered Chains. *J. Phys. Chem.* **1982**, *86*, 5145−5150.

(71) Macphail, R. A.; Strauss, H. L.; Snyder, R. G.; Elliger, C. A. C−H Stretching Modes and the Structure of *n*-Alkyl Chains. 2. Long, All-Trans Chains. *J. Phys. Chem.* **1984**, *88*, 334−341.

(72) Stevens, M. J. Thoughts on the Structure of Alkylsilane Monolayers. *Langmuir* **1999**, *15*, 2773−2778.

(73) Offord, D. A.; Griffin, J. H. Kinetic Control in the Formation of Self-Assembled Mixed Monolayers on Planar Silica Substrates. *Langmuir* **1993**, *9*, 3015−3025.

(74) Collman, J. P.; Devaraj, N. K.; Eberspacher, T. P. A.; Chidsey, C. E. D. Mixed Azide-Terminated Monolayers: A Platform for Modifying Electrode Surfaces. *Langmuir* **2006**, *22*, 2457−2464.

(75) Andrews, S. S.; Boxer, S. G. Vibrational Stark Effects of Nitriles I. Methods and Experimental Results. *J. Phys. Chem. A* **2000**, *104*, 11853−11863.

(76) Hush, N. S.; Reimers, J. R. Vibrational Stark Spectroscopy. 1. Basic Theory and Application to the CO Stretch. *J. Phys. Chem.* **1995**, *99*, 15798−15805.

(77) Levinson, N. M.; Fried, S. D.; Boxer, S. G. Solvent-Induced Infrared Frequency Shifts in Aromatic Nitriles Are Quantitatively Described by the Vibrational Stark Effect. *J. Phys. Chem. B* **2012**, *116*, 10470−10476.

(78) Williams, R. B.; Loring, R. F.; Fayer, M. D. Vibrational Dephasing of Carbonmonoxy Myoglobin. *J. Phys. Chem. B* **2001**, *105*, 4068−4071.

(79) Geissler, P. L. Water Interfaces, Solvation, and Spectroscopy. *Annu. Rev. Phys. Chem.* **2013**, *64*, 317−337.

(80) Corcelli, S.; Lawrence, C. P.; Skinner, J. L. Combined Electronic Structure/Molecular Dynamics Approach for Ultrafast Infrared Spectroscopy of Dilute HOD in Liquid H_2O and D_2O. *J. Chem. Phys.* **2004**, *120*, 8107−8117.

(81) Nishida, J.; Fayer, M. D. Theory of Third-Order Spectroscopic Methods To Extract Detailed Molecular Orientational Dynamics for Planar Surfaces and Other Uniaxial Systems. *J. Chem. Phys.* **2014**, *140*, 144702.

(82) Angst, D. L.; Simmons, G. W. Moisture Absorption Characteristics of Organosiloxane Self-Assembled Monolayers. *Langmuir* **1991**, *7*, 2236−2242.

(83) Merchant, K. A.; Noid, W. G.; Akiyama, R.; Finkelstein, I.; Goun, A.; McClain, B. L.; Loring, R. F.; Fayer, M. D. Myoglobin-CO Substate Structures and Dynamics: Multidimensional Vibrational Echoes and Molecular Dynamics Simulations. *J. Am. Chem. Soc.* **2003**, *125*, 13804−13818.

(84) Pfalzgraff, W. C.; Markland, T. E. Private communication, 2015.